RSC Advances

RSC Advances

www.rsc.org/advances

ROYAL SOCIETY OF CHEMISTRY

www.rsc.org/advances

RSC Advances
RSC**Publishing**

PAPER

Flexible and enhanced thermal conductivity of Al$_2$O$_3$@Polyimide hybrid film *via* coaxial electrospinning

Jianwen Xia,[ab] Guoping Zhang, [a,c]* Libo Deng, [a] Haipeng Yang, [b] Rong Sun, [a]* and Ching-Ping Wong[a,c]

A novel core-shell structure of Al$_2$O$_3$ nanoparticles (NPs) attached on poly (amic acid) (PAA) fiber has been successfully developed by facile coaxial electrospinning technology for the first time. The as-prepared PAA fiber went through imidization to prepare Al$_2$O$_3$@polyimide (Al$_2$O$_3$@PI) film. The resultant films with different Al$_2$O$_3$ contents are characterized by scanning electron microscopy, Fourier transform infrared spectroscopy, thermal gravimetric analysis, and dynamical mechanical analysis, respectively. The results indicated that the Al$_2$O$_3$ NPs could uniformly decorate the surface of fibers with a diameter of about 1 μm which enhanced thermal and mechanical properties of fiber-based film. Especially for the flexible film with the content of Al$_2$O$_3$ as high as 59.3 wt%, it presents a high storage modulus (2.11GPa) and excellent thermal stability (474 ^{o}C at 5% mass loss) as well as superior thermal conductivity of 9.66 Wm^{-1}K^{-1} in plane. At last, compared with pure PI film, the Al$_2$O$_3$@PI fiber-based film exhibits excellent thermal transfer ability in the light emitting diode packaging. Therefore, the novel Al$_2$O$_3$@PI fiber-based film with integrated properties of insulation, thermal conductivity and flexibility can be used for wearable electronics and power devices.

Introduction

With the progress in size and performance of electronic devices which become denser and more powerful rapidly, the continued miniaturization of electronic device components requests higher heat dissipation. There is no doubt that the operating temperature of the junction has exponentially affected the reliability of an electronic device[1]. Thus, developing high thermal conductivity materials to dissipate unwanted heat quickly and effectively is desirable.[2] Comparing with low-melting-point solder alloy, polymer based composites with good adhesion to various substrates, economic and excellent processing performance have attracted a great deal of interests in the field of electronic packaging[3, 4]. However, the thermal conductivity of polymer is usually in the order of 0.2 Wm^{-1}K^{-1}. To overcome this problem, various conductive materials, such as Ag[5], graphene[6], carbon nanotube[7], graphite[8] are used as thermal transfer medium to fill them into polymer matrix. Though these fillers can increase thermal conductivity in certain extent, they cause target composites to be electrically conductive simultaneously[9]. On the other hand, high thermal conductive materials with electrically insulation are much more significant and meet the special demand of electronic packaging. Thus, some ceramic fillers including boron nitride[10, 11], aluminum nitride[12], silicon carbide[13], and alumina (Al$_2$O$_3$)[14],

etc, are used as high thermal conductive fillers to blend with polymer substrate. It is well known that a high volume fraction of thermally conductive fillers, generally >60 vol%[1], is necessary to obtain high thermal conductivity for the composite. However, such high contents of inorganic fillers would consequentially disserve the mechanical property and flexibility of polymer composite to limit its practical application. Furthermore, the thermal conductivity of composite is lower than expected because of high thermal resistance at the interface between the filler and the resin.[15] Therefore, developing novel composites with high thermal conductivity and mechanical property are still a challenge.

Among the polymer fiber fabrication methods, electrospinning has emerged as an attractive technique for the preparation of an array of merits of the ultrafine fibers in micro/nano-scale fineness[16]. The as-prepared materials with functional architecture have been exploited for diverse applications like filtration, nano-sensors, tissue engineering, and so on[17]. Many technologies such as so-gel[18], radio frequency sputtering[19], metal-organic chemical vapor deposition[20] and atomic layer deposition[21] have been reported for electrospinning inorganic nanofibers to obtain inorganic-inorganic core-shell or hierarchical nanostructure[22-25] for its various functional properties. However, the fabrication of polymer-inorganic core-shell nanofibers is somewhat challenging because the deposition of inorganic shell layer

requires a high temperature process that leads to the degradation of polymeric core structure easily. Very recently it emerged that the coaxial electrospinning technology provided an alternative route to design functional composite with core-shell or hollow structures[26-29]. Therefore, the coaxial electrospinning become a kind of very promising technique for preparing functional composite material. Nevertheless, to the best of our knowledge, the focus on the fabrication of polymer-inorganic core-shell nanofibers directly by coaxial electrospinning has been very limited in the literature[16].

Herein, we demonstrate a novel and simple approach to coat Al_2O_3 nanoparticles (NPs) onto PI fiber (denoted as Al_2O_3@PI) by coaxial electrospinning as shown in Fig.1. Firstly, under proper voltage, polyvinylpyrrolidone (PVP) solution including Al_2O_3 NPs and poly (amic acid) (PAA) was sprayed through a coaxial spinneret simultaneously and the resultant composite fibers were collected by rotating collector with much higher speed for orientation. Secondly, the resultant film was cured to prepare Al_2O_3@PI composite fiber-based film. The fibers were oriented to maximize the conductivity, and the Al_2O_3 NPs coated on the fiber further provided much more thermal conductive paths in plane. Furthermore, the structure, morphology, thermal conductivity and mechanical properties of the as-prepared hybrid film were comprehensively investigated. At last, the practical thermal transfer performance was also investigated in the light emitting diode (LED) packaging.
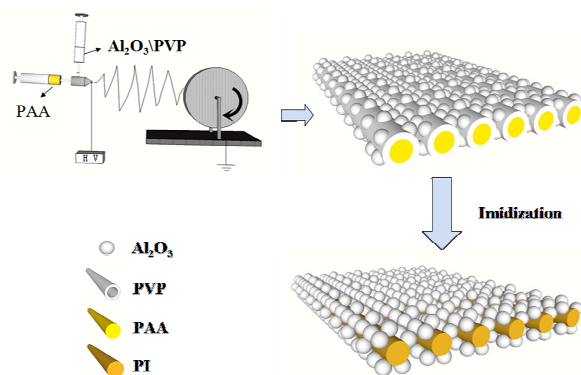

Fig. 1 Schematic illustration for the fabrication of Al_2O_3@PI composite fiber-based film.

Experimental

Materials

Pyromellitic dianhydride (PMDA), 4, 4'-oxidianiline (ODA) and N, N-dimethylacetamide (DMAc) were commercially obtained from China National Medicine Co. PVP was supplied by Aladdin. The Al_2O_3 NPs with an average diameter of 200 nm were supplied by Denki Kagaku Kogyo Kabushiki Kaisha, Japan. The commercial thermal conductive glue ST922 was commercially supplied by Balance Stars Co., LTD.

Preparation of precursor solutions

The precursor PAA was synthesized by the reaction between ODA and PMDA with an equivalent molar ratio. The polycondensation was performed in DMAc at about 0 °C for 4 hours. The solid content of the pristine PAA solution was 15 wt%. The as-prepared PAA solution was directly used as the

core component in coaxial electrospinning. As the shell component, the typical procedure of preparing PVP solution including Al_2O_3 NPs was operated as follows. Firstly, the Al_2O_3 fine powder was fully dispersed in DMAc by ultrasonic for 4 hours. Then appropriate PVP was added into the solution under magnetic stirring until dissolved completely.

Coaxial electrospinning

Coaxial electrospinning equipment (SS3556H) was supplied by Beijing Ucalery Technology and Development Co., Ltd. The PVP solution and PAA solution were poured into 10 mL plastic syringes mounted on the pump with a multitrack grip, respectively. Hence, the flow rates of two kinds of solutions were identical during the process. The coaxial spinneret was comprised of an inner needle (inner diameter = 0.50 mm and outer diameter = 0.80 mm) concentrically mounted on an outer needle (i.d 1.26 mm, o.d. 1.66 mm) and was grounded by use of an alligator clip. Then electrospinning was carried out at an applied voltage of 15-20 kV. The feeding rate of each syringe was 0.60 mL h^{-1} and the spinneret-collector distance was 20 cm. Herein, by adjusting the concentrations of Al_2O_3 NPs in PVP, different contents Al_2O_3 NPs, including 0, 26.7, 42.2, 59.3, 74.5 wt%, of PAA composite fibers could be attained. Then all the electrospun fiber-based films were dried at 60 °C overnight to evaporate completely the residual solvent. And thermally imidization was completed by the following program: heated at 150 °C for 60 min, 270 °C for 60 min and 300 °C for 180 min with a heating rate of 5 °C min^{-1}.

Characterization of composites

The morphology of as-prepared fibers was studied by scanning electron microscopy (SEM), which was recorded with a Nova NanoSEM 450. The weight losses of the composites were analyzed using thermal gravity analysis (TGA) which was made on a TA SDTQ600 thermo-gravimetric analyzer. The microbalance has a precision of ±0.1 μg. Samples of about 10 mg were placed into 70 μL alumina pans. The samples were heated from 30 to 800 °C under an air flow of 100 mL min^{-1}. Fourier transform infrared (FTIR) spectra were recorded with Bruker Vertex 70 spectrometer (Bruker Optik GmbH, Ettlingen, Germany) in the range of 4000–400 cm^{-1}. The thermal diffusivity of the composites was investigated at 25 °C through xenon flash equipment (LFA447, Germany) according to ASTM E1461. The diameter of sample used for laser flash method was 1 inch and a thickness of 50±5 μm with the mirror-like polished surface. Differential scanning calorimetry (DSC) with sapphire reference was used to measure the specific heat capacity (Cp) with a heating rate of 5 °C min^{-1} under nitrogen. The density of composites was measured by the Archimedean buoyancy method using an electronic analytical balance (FA2104J, China).

Tensile test property of PI composites samples at room temperature was measured using dynamical mechanical analysis (DMA, Q800, TA instruments) with stress-strain model. The force was raised at the rate of 1N min^{-1} to 18 N.

The samples were cut in rectangle about 5 mm × 50 mm, with a thickness about 50 μm which measure by micrometer at five different points for each sample. And each point was measured for three times. FLIR-T355 infrared camera was used to take picture for the temperature field of LED at room temperature (24 °C) with relative humidity of 56%, and the measurement distance between the lens and the target was 0.2 m.

Results and Discussion

Characterization of Al₂O₃@PI fiber-based film

Polyimide was used as the core layer of composite fiber due to its thermal stability and conventional use in microelectronic applications. Different contents of Al_2O_3 NPs were used as the thermal transfer medium in this design because of their excellent thermal conductivity and high filler contents. By controlling the electrospun polymer solution and the electrospinning conditions (e.g., voltage, speed), we can obtain highly aligned fibers with uniform diameter (about 1μm) after imidization, as shown in Fig. 2. With increasing of Al_2O_3 contents from 26.7 wt% to 74.5 wt% in the composite fiber, the Al_2O_3 NPs located on the shell layer become denser and cover the whole surface of fiber.
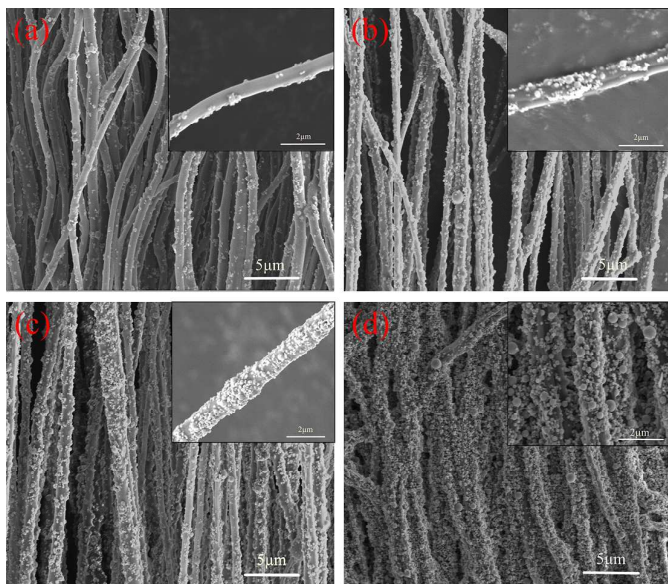

Fig. 2 SEM images of PI fibers with Al_2O_3 NPs contents of (a) 26.7 wt%, (b) 42.2 wt%, (c) 53.9 wt% and (d) 74.5 wt%.

The uniform dispersion of the Al_2O_3 NPs in the composites is an important issue for the functional material. Thus, PVP was used to prepare stable solution including Al_2O_3 NPs not only it conducive to the dispersion of inorganic filler[30, 31] but also it is a template for preparing PAA fibers[32]. However, to realize the thermal conductivity of composite fiber film, the PVP shell layer should be removed to expose the Al_2O_3 NPs. It can be seen that in the Al_2O_3@PAA composite fiber with a PVP coating layer, most of the Al_2O_3 NPs were covered by PVP and the fiber surface was very smooth (Fig. S1). Then, during high-temperature imidization process, the PVP in the shell layer was

removed and much more Al_2O_3 spherical NPs with content of 74.5 wt% could be exposed and evenly distributed over the surface of the fibers as shown in Fig. 2d. Therefore, the PVP can be facilely removed to decrease the interfacial thermal resistance of composite fiber-based film.

To characterize the structure variations during the process of imidization of composite, FT-IR spectra were recorded in Fig. 3 and Fig. S2. It can be seen that the characteristic peaks at 1662, 1442 and 1296 cm⁻¹ were attributed to the stretching vibration of carboxide (C=O), C-H bending vibration and stretching vibration of PVP, respectively, as shown in Fig. S2. These characteristic peaks also presented in the samples before curing as shown in Fig. 3a-c which disappeared after imidization (Fig. 3d), indicating that PVP could be removed completely in the as-prepared composite fiber. Furthermore, in the curve of composite fiber, the characteristic peaks at 1780 cm⁻¹, 1730 cm⁻¹ and 723 cm⁻¹, as shown in Fig. 3d, were attributed to asymmetric vibration, symmetric vibration and bending vibration of carboxide (C=O) of PI respectively[5, 33], indicating that the PI fibers coated by Al_2O_3 NPs have been successfully prepared according to the proposed imidization procedure.
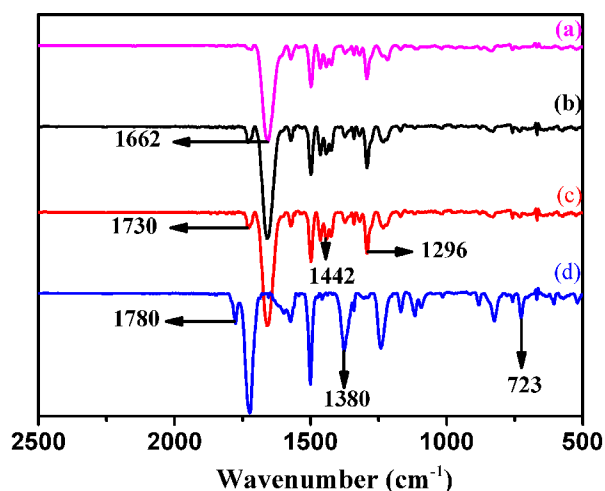

Fig. 3 FTIR spectra of composite fiber-based film at different stages during imidization: (a) room temperature, (b) after 150 °C for 1 hour, (c) after 270 °C for 1 hour and (d) after 300 °C for 3 hours.

Mechanical properties of Al₂O₃@PI fiber-based film

It was expected that the mechanical properties of the composite fiber would be enhanced due to the large aspect ratio of Al_2O_3 NPs, strong adhesion between Al_2O_3 NPs and PI fiber. The typical tensile stress-strain curves of Al_2O_3@PI fiber-based films are shown in Fig. 4 and summarized in Table 1. The oriented pure PI fiber-based film exhibits a remarkable tensile strength of 16.13 MPa and the elongation at the break is 2.67%. From the slope of the stress-strain curve, the elastic modulus was measured, which is 0.81 GPa for pure PI film, in the order of that of pure PI polymer as reported[34, 35]. As shown in Table 1, with the increase of Al_2O_3 contents, the elastic modulus of

the composites was increased when the Al$_2$O$_3$ content was below than 59.3 wt%. However, the elastic modulus of Al$_2$O$_3$@PI fiber-based film with 74.5 wt% of Al$_2$O$_3$ was reduced which indicated that the inorganic particles with higher contents may deteriorate the mechanical performance of the composites, which was consistent with previous work[36, 37]. This might be related to poor dispersion of Al$_2$O$_3$ NPs in the PI matrix. The decrease of the tensile strength could be caused by the premature failure starting at the filler aggregates[38]. In our work, the Al$_2$O$_3$@PI fiber-based film with high contents (59.3 wt%) of inorganic particles possessed higher elastic modulus (2.11 GPa) than those of pure PI film, which also has excellent flexibility as shown in Fig. 4b. After crimping and bending, there was no crack generated. Therefore, the composites with high inorganic filler contents were prepared by coaxial electrospinning. Such high loadings endow the fibers with high mechanical strength as well as excellent flexibility.
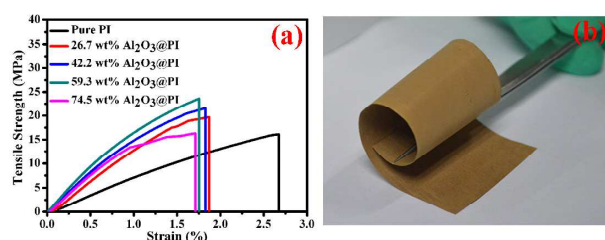

Fig. 4 (a) Stress–strain curves of pure PI and Al$_2$O$_3$@PI fiber-based films and (b) the photograph of Al$_2$O$_3$@PI fiber-based film with 59.3 wt% of Al$_2$O$_3$ NPs under winding condition.

Table 1 Mechanical and thermal properties of the Al$_2$O$_3$@PI fiber-based films

Al$_2$O$_3$ (wt%)	Tensile strength (MPa)	Elongation (%)	Elastic modulus (GPa)	T_5 (°C)
0	16.13	2.67	0.81	420
26.7	19.71	1.87	1.53	430
42.2	21.58	1.83	1.85	437
59.3	23.62	1.75	2.11	474
74.5	16.28	1.71	1.74	517

Thermal properties of Al$_2$O$_3$@PI fiber-based films

The thermal stability of pure PI and Al$_2$O$_3$@PI fiber-based films were assessed as shown in Fig. 5. The temperature corresponding to 5% weight loss (T_5) was taken as an index of thermal stability as shown in Table 1. It can be seen that the decomposition of pure PI and Al$_2$O$_3$@PI fiber-based films took place in a single step and it started at around 420 °C. From the inset we can see that the T_5 of composites shifted to an obvious higher temperature with the increase of Al$_2$O$_3$ contents compared with that of pure PI. The T_5 of 59.3 wt% Al$_2$O$_3$@PI film increased by 54 °C and up to 474 °C comparing to that of pure PI film. Therefore, these results suggested that the immobilization of Al$_2$O$_3$ NPs could enhance the thermal stability of composite films.
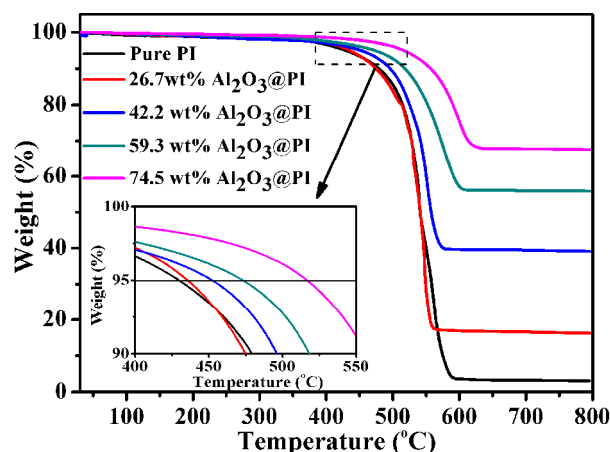

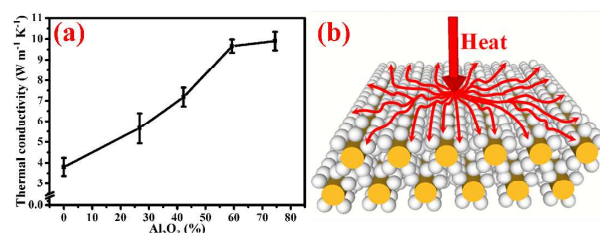Fig. 5 TGA curves of pure PI and Al$_2$O$_3$@PI fiber-based films.

Fig. 6 (a) The thermal conductivity of Al$_2$O$_3$@PI fiber-based film with different contents of Al$_2$O$_3$ NPs and (b) one probable thermal transfer model in the Al$_2$O$_3$@PI fiber-based film.

It is recognized that the key to improve the thermal conductivity of a resin is the formation of effective thermal conductivity network in matrix. In present work, oriented fibers may improve the thermal conductivity of composites along the axial direction. Furthermore, the dense spherical Al$_2$O$_3$ NPs decorated on the whole surface of separate PI fiber would provide much more thermal conductivity channels in plane. Then, the thermal conductivity can be calculated using the definition of diffusivity

$$\alpha = k \cdot \rho^{-1} C_p^{-1} \qquad (1)$$

where k is the thermal conductivity, ρ is the density and C_p is the specific heat at constant pressure as shown in Table S1. The thermal conductivities of composites with different contents of Al$_2$O$_3$ were determined using Eq. (1) and shown in Fig. 6a. The pure PI film showed high thermal conductivity of 3.80 W m^{-1} K^{-1}, which can be explained by the high orientation of the fiber as reported[39, 40]. Furthermore, the thermal conductivity of composite films increased sharply with increasing Al$_2$O$_3$ contents from 0 to 59.3 wt%. With the densely decorating of the Al$_2$O$_3$ NPs in the alignment PI fiber which form effective conductive paths or network to improve the thermal diffusion ability in plane as shown in Fig. 6b. When the content of Al$_2$O$_3$ was increased up to 59.3 wt%, the composite film showed excellent thermal conductivity of 9.66 W m^{-1} K^{-1}, while the

thermal conductivity of composite film with 74.5 wt% Al_2O_3 was 9.90 W m^{-1} K^{-1} by the increment of 2.5%. Therefore, the enhanced thermal conductive composite film with core-shell structure was developed by coaxial electrospinning technology facilely.

To validate the practical application of the as-prepared Al_2O_3@PI fiber-based film in electronic device, LED was used as a typical heat source and placed at the center of the film sample with 59.3 wt% of Al_2O_3 NPs and bonded by commercial thermal conductive glue (ST922). By recording the changing of temperature of LED, the thermal diffusion ability of different films could be qualitatively compared. For reducing the error, the same amount of glue was used for packing the LED on the sample with Cu wire to connect the power supply. The size of film sample was 1 inch with 50 um of thickness as shown in Fig. 7. In order to imaging the temperature field of the thermal source during LED working, FLIR T335 infrared camera was used. With a thermal sensitivity of 0.05 ^{o}C and high speed data acquisition and evaluation of thermal images, it makes up an excellent investigative tool to analysis of the high-frequency temperature fields. Different voltages were used to investigate the thermal transfer property of pure PI and composite films as shown in Fig. 8. It depicts that temperature distribution of packaging just after the end of heating time t_h (t_h=300s, U=3.2, 3.4 V). The stable temperature of composite and pure PI film under 3.2 V were in the order of 41.6, 45.7 ^{o}C, respectively, and under 3.4 V were about 85.4, 97.7 ^{o}C, respectively. It's worth noting that the thermal conductivity of the glue was 0.671 W m^{-1} K^{-1}, and which could not diffuse the heat flow from LED to the film effectively. Therefore, there was not any significant improvement for PI composite film. However, it can be found that the composite film had comparative thermal transfer ability compared with that of pure PI film by infrared camera. Meanwhile, the LED packaging based on composite film possesses much broader thermal stream distribution than that of pure PI film. Furthermore, when the loaded voltage and heating time were the same, the temperature of LED packed on Al_2O_3@PI fiber-based film was always lower than that of LED packed on pure film as shown in Fig. 9, which suggested that the composite film possessed excellent thermal diffusion rate in plane.
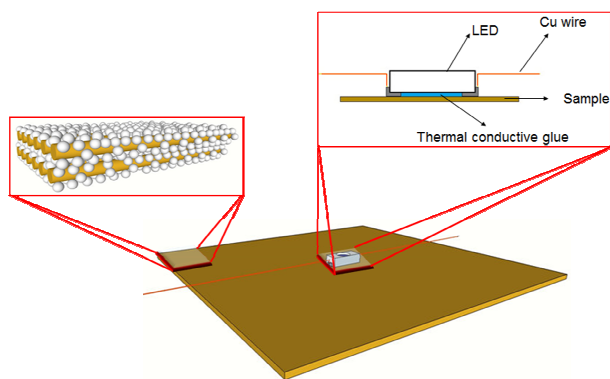
Fig. 7 Schematic depicting the LED packed with Al_2O_3@PI fiber-based film
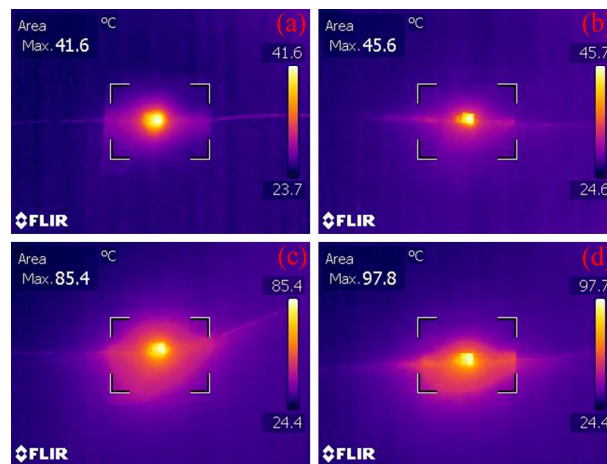

Fig. 8 Local temperature of LED packaging under different voltages after 300 s: (a, b) 59.3 wt% Al_2O_3@PI fiber-based film and pure PI film under 3.2 V, (c, d) 59.3 wt% Al_2O_3@PI fiber-based film and pure PI film under 3.4 V.
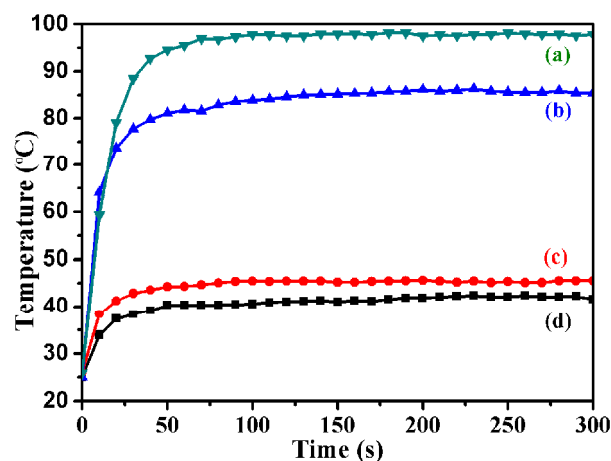

Fig. 9 The temperature of LED packed by different films varying with times under different voltage: (a, b) Pure PI film and 59.3 wt% Al_2O_3@PI film under voltage of 3.4 V, (c, d) Pure PI film and 59.3 wt%Al_2O_3@PI film under voltage of 3.2 V.

Conclusions

In summary, a novel Al_2O_3@PI fiber-based film was successfully developed by a facile coaxial electrospinning technology for the first time. Thereinto, the Al_2O_3 NPs can be coated on the separate PI fiber densely when the contents of Al_2O_3 rose up to 59.3 wt%, which still exhibited remarkably high elastic modulus (2.11 GPa), flexibility and enhanced thermal conductivity (9.66 W m^{-1} K^{-1}). Furthermore, the specific composite film was used as a thermal dissipation material in the LED packaging. The results indicated that the

as-prepared Al$_2$O$_3$@PI fiber-based film could disperse unwanted heat effectively and rapidly compared with pure PI film. Therefore, the present material and process design may provide a novel platform for the synthesis of other multifunctional composites for various special applications.

Acknowledgements

Notes and references

^{a}Shenzhen College of Advanced Technology, University of Chinese Academy of Sciences, Shenzhen 518055, China

E-mail: gp.zhang@siat.ac.cn

^{b}College of Materials Science and Engineering, Shenzhen University, Shenzhen, 518060, China

^{c}School of Materials Science and Engineering, Georgia Institute of Technology, 771 Ferst Drive, Atlanta, Georgia, 30332, United States

Corresponding author：Guoping Zhang (gp.zhang@siat.ac.cn) and Rong Sun (rong.sun@siat.ac.cn)

1 Y. Hwang, M. Kim and J. Kim, *RSC Adv.*, 2014, **4**, 17015.
2 V. Singh, T. L. Bougher, A. Weathers, Y. Cai, K. Bi, M. T. Pettes, S. A. McMenamin, W. Lv, D. P. Resler, T. R. Gattuso, D. H. Altman, K. H. Sandhage, L. Shi, A. Henry and B. A. Cola, *Nat. Nanotechnol*, 2014, **9**, 38 4-390.
3 Y. Zhou, Y. Yao, C. Y. Chen, K. Moon, H. Wang and C. P. Wong, *Sci., Rep.*, 2014, **4**, 4779.
4 C. Min, D. Yu, J. Cao, G. Wang and L. Feng, *Carbon*, 2013, **55**, 116-125.
5 C. Zandén, X. Luo, L. Ye and J. Liu, *Compos. Sci. Technol.*, 2014, **94**, 54-61.
6 R. Qian, J. Yu, C. Wu, X. Zhai and P. Jiang, *RSC Adv.*, 2013, **3**, 17373.
7 Z. Han and A. Fina, *Prog. Polym. Sci.,* 2011, **36**, 914-944.
8 M. T. Pettes, H. Ji, R. S. Ruoff and L. Shi, *Nano Lett.*, 2012, **12**, 2959-2964.
9 R. Qian, J. Yu, C. Wu, X. Zhai and P. Jiang, *RSC Adv.*, 2013, **3**, 17373.
10 T. L. Li and S. L.C. Hsu, *J. Mater. Chem. B*, 2010, **114**, 6825.
11 W. Yan, Y. Zhang, H. Sun, S. Liu, Z. Chi, X. Chen and J. Xu, *J. Mater. Chem. A*, 2014, **2**, 20958-20965.
12 A. Agrawal and A. Satapathy, *Compos. Part A-Appl S.*, 2014, **63**, 51-58.
13 J. P. Cao, X. Zhao, J. Zhao, J. W. Zha, G. H. Hu and Z. M. Dang, *ACS Appl. Mater. Interfaces*, 2013, **5**, 6915-6924.
14 Z. Li, W. Wu, H. Chen, Z. Zhu, Y. Wang and Y. Zhang, *RSC Adv.*, 2013, **3**, 6417.
15 Y. Shimazaki, F. Hojo and Y. Takezawa, *Appl. Phys. Lett.*, 2008, **92**, 133309.
16 F. Kayaci, C. Ozgit-Akgun, I. Donmez, N. Biyikli and T. Uyar, *ACS Appl. Mater. Interfaces*, 2012, **4**, 6185-6194.
17 H. Yuan, S. Zhao, H. Tu, B. Li, Q. Li, B. Feng, H. Peng and Y. Zhang, *J. Mater. Chem.*, 2012, **22**, 19634.
18 Y. Aykut, C. D. Saquing, B. Pourdeyhimi, G. N. Parsons and S. A. Khan, *ACS Appl. Mater. Interfaces*, 2012, **4**, 3837-3845.
19 L. Liu, H. Zhang, Y. Wang, Y. Su, Z. Ma, Y. Xie, H. Zhao, C. Chen, Y. Liu, X. Guo, Q. Su and E. Xie, *Nanoscale Res. Lett.*, 2010, **5**, 1418-1423.
20 M. E. Fragalà, I. Cacciotti, Y. Aleeva, R. Lo Nigro, A. Bianco, G. Malandrino, C. Spinella, G. Pezzotti and G. Gusmano, *CrystEngComm*, 2010, **12**, 3858.
21 S. W. Choi, J. Y. Park and S. S. Kim, *Nanotechnology*, 2009, **20**, 465603.
22 S. H. Ahn, D. J. Kim, W. S. Chi and J. H. Kim, *Adv. Mater.*, 2013, **25**, 4893-4897.
23 Y. Zhang, R. Li, X. Zhou, M. Cai and X. Sun, *Cryst. Growth Des.*, 2009, **9**, 4230-4234.
24 N. Wang, C. Sun, Y. Zhao, S. Zhou, P. Chen and L. Jiang, *J. Mater. Chem.*, 2008, **18**, 3909.
25 X. Wang, D. P. Yang, P. Huang, M. Li, C. Li, D. Chen and D. Cui, *Nanoscale*, 2012, **4**, 7766-7772.
26 T. Yuan, B. Zhao, R. Cai, Y. Zhou and Z. Shao, *J. Mater. Chem.*, 2011, **21**, 15041.
27 Q. Ma, J. Wang, X. Dong, W. Yu, G. Liu and J. Xu, *J. Mater. Chem.*, 2012, **22**, 14438.
28 H. Yang, C. R.Lightner and L. Dong, *ACS Nano*, 2012, **6**, 622-628.
29 M. Pakravan, M. C. Heuzey and A. Ajji, *Biomacromolecules*, 2012, **13**, 412-421.
30 G. Chang, L. He, W. Zheng, A. Pan, j. Liu, Y. Li and R. Cao, *J Colloid Interf. Sci.*, 2013, **396**, 129-137.
31 S. P. Bhardwaj, K. K. Arora, E. Kwong, A. Templeton, S. D. Clas and R. Suryanarayanan, *Mol. Pharm.*, 2014, **11**, 4228-4237.
32 C. Li, Z. H. Wang, D. G. Yu and G. R. Williams, *Nanoscale Res. Lett.*, 2014, **9**, 258.
33 D. Chen, Y. E. Miao and T. Liu, *ACS Appl. Mater. Interfaces*, 2013, **5**, 1206-1212.
34 I. H. Tseng, J. C. Chang, S. L. Huang and M. H. Tsai, *Polym. Int.*, 2013, **62**, 827-835.
35 J. H. Seol, J. H. Won, M. S. Lee, K. S. Yoon, Y. T. Hong and S. Y. Lee, *J. Mater. Chem.*, 2012, **22**, 1634.
36 S. Zhao, L. Schadler, H. Hillborg and T. Auletta, *Compos. Sci. Technol.*, 2008, **68**, 2976-2982.
37 L. Fang, C. Wu, R. Qian, L. Xie, K. Yang and P. Jiang, *RSC Adv.*, 2014, **4**, 21010.
38 H. Liimatainen, N. Ezekiel, R. Sliz, K. Ohenoja, J. A. Sirvio, L. Berglund, O. Hormi and J. Niinimaki, *ACS Appl. Mater. Interfaces*, 2013, **5**, 13412-13418.
39 Y. Liu and S. Kumar, *ACS Appl. Mater. Interfaces*, 2014, **6**, 6069-6087.
40 G. Yuan, X. Li, Z. Dong, A. Westwood, B. Rand, Z. Cui, Y. Cong, J. Zhang, Y. Li, Z. Zhang and J. Wang, *Carbon*, 2014, **68**, 426-439.